IOP Conf. Series: Journal of Physics: Conf. Series **868** (2017) 012019 doi:10.1088/1742-6596/868/1/012019

Drastic effect of the Mn-substitution in the strongly correlated semiconductor $FeSb_2$.

Mohamed A. Kassem*, Yoshikazu Tabata, Takeshi Waki, Hiroyuki Nakamura.

Department of Materials Science and Engineering, Kyoto University, Kyoto 606-8501, Japan.

E-mail: kassem.ahmed.82s@st.kyoto-u.ac.jp

Abstract. We report the effects of Mn substitution, corresponding to hole doping, on the electronic properties of the narrow gap semiconductor, $FeSb_2$, using single crystals of $Fe_{1-x}Mn_xSb_2$ grown by the Sb flux method. The orthorhombic *Pnnm* structure was confirmed by powder X-ray diffraction (XRD) for the pure and Mn-substituted samples. Their crystal structure parameters were refined using the Rietveld method. The chemical composition was investigated by wavelength-dispersive X-ray spectroscopy (WDX). The solubility limit of Mn in $FeSb_2$ is $x_{max} \sim 0.05$ and the lattice constants change monotonically with increasing the actual Mn concentration. A drastic change from semiconducting to metallic electronic transports was found at very low Mn concentration at $x \sim 0.01$. Our experimental results and analysis indicate that the substitution of a small amount of Mn changes drastically the electronic state in $FeSb_2$ as well as the Co-substitution does: closing of the narrow gap and emergence of the density of states (DOS) at the Fermi level.

1. Introduction

Strongly correlated electron materials have unusual electronic structures and show interesting properties, such as metal-insulator transitions, heavy fermions, narrow-gap semiconductors and high-T_c superconductivity. Among of them, the narrow-gap semiconductors, such as Kondo semiconductors are characterized by a narrow gap at the Fermi level and sharp DOS peaks near the Fermi level due to the electron correlations and hybridization between broad conduction electron bands and narrow *d*- or *f*-electron bands [1].

FeSi and $FeSb_2$ are a few candidates of *d*-electron based electron-correlation driven semiconductors [1,2]. In recent years considerable attention has been paid for studying $FeSb_2$ because of its anomalously huge Seebeck coefficient [3]. $FeSb_2$ crystallizes in the marcasite crystal structure of orthorhombic space group *Pnnm* with lattice parameters of $a = 5.8328(5)$, $b = 6.5376(5)$ and $c = 3.1973(3)$ Å [4]. Fe-atom at (0, 0, 0) is octahedrally surrounded by Sb atoms at (x, y, 0) and the $FeSb_6$ octahedra forms edge-shared chains along the *c* axis. Two-energy-gap behavior in resistivity and thermally activated Pauli paramagnetic behavior were experimentally observed in single crystals of $FeSb_2$ [5,6]. Evolution of ferromagnetic ground state and gap closing were reported by the substitution of a small amount of third element, for instance, by substituting Co for Fe and Te for Sb [7,8]. The high sensitivity on its transport and magnetic properties against element substitutions is important to understand the nature of the narrow-gap semiconducting state of $FeSb_2$ because it can be explained based on the electron-correlation driven mechanism.

* Permanent Address: Department of Physics, Assiut University, Assiut 71515, Egypt

In this paper we report on the Mn-substitution effects on the electronic transport properties of $FeSb_2$, which is a counterpart of the Co-substitution effects: the former is a hole doping and the latter is an electron doping. The systematic substitution of Mn for Fe and its solubility limit were investigated by XRD and SEM-WDX for pure and doped samples. The electrical resistivity measurements show drastic changes in the electronic state and gap closing in $Fe_{1-x}Mn_xSb_2$. Interestingly, the energy gap is much more sensitive to the Mn-substitution than the Co-substitution.

2. Experimental Details

Silver rod-shaped single crystals of $Fe_{1-x}Mn_xSb_2$ with the long axis parallel to the *b* axis were synthesized by the high temperature self Sb-flux method. The grown crystals were characterized by powder XRD at room temperature (PANalytical, X'Pert Pro) with Cu$K_{\alpha 1}$ radiation monochromated by a Ge (111)-Johansson-type monochromator. The crystal structure parameters were refined by the Rietveld analysis using TOPAS (Bruker) [9]. To identify the actual Mn concentrations in the grown crystals, the chemical compositions were investigated by SEM-WDX (Hitachi, S-3500H). The actual Mn-concentrations measured by the WDX were found to be considerably reduced from the nominal starting concentrations. The WDX results also indicated the solubility limit of $x_{max} \approx 0.05$. The crystalline axes were determined by the X-ray Laue method. The susceptibility of the parent compound, $FeSb_2$, was measured using a SQUID magnetometer (Quantum Design, MPMS-7) in a temperature range of T = 2 - 350 K by applying magnetic field along the three axes. Unfortunately, a very small amount of ferromagnetic impurity with $T_C \sim 150$ K, which is too small to be detected by any other techniques, masks the intrinsic susceptibility in the Mn-substituted $Fe_{1-x}Mn_xSb_2$. Hence, we do not discuss the magnetic properties except for pure $FeSb_2$. Electrical resistivity was measured by the four probe method of rectangular rods of single crystals cut along the three principal crystal axes in a temperature range of T = 4 - 300 K.

3. Results and Discussions

The phase and the crystal structure are investigated by powder XRD using powders crushed from the crystals. The observed diffraction patterns are fitted by the Rietveld method using the structure parameters of $FeSb_2$ marcasite structure of *Pnnm* orthorhombic symmetry. Both observed and calculated XRD patterns of $Fe_{1-x}Mn_xSb_2$ at room temperature as well as the differences are shown in Fig. 1. The main phase of the obtained crystals for all Mn concentrations is $FeSb_2$ phase. Figure 2 shows the refined lattice parameters *a, b* and *c* (Fig. 2a) and the unit cell volume *V* (Fig. 2b) plotted against Mn concentration *x*. The lattice parameters as well as unit cell volume increase linearly as *x* increasing and obey well the Vegard's law indicating successful substitution of Mn for Fe in $Fe_{1-x}Mn_xSb_2$. The crystal structure parameters with the reliability *R*-factors and goodness-fit-indicator *S* for different Mn concentrations are listed in Table 1. The Fe/Mn occupancies were fixed based on the WDX results. The low values of *S* and *R*-factors indicate the satisfactory refinement.

Figure 3 shows the temperature dependences of the magnetic susceptibility M/H of $FeSb_2$ single crystals with H parallel to the three principal crystal axes, where M is the magnetization and H is the applied magnetic field. A thermally activated behavior was found as well as previous reports [2,6]. Upturns at low T are attributed to small amounts of magnetic impurities. Following the previous reports [6,7], we analyze the temperature dependence of the magnetic susceptibility based on the narrow-band small-gap model with a density of states $N(E)$ consisting of two narrow bands of the width W separated by a gap $E_g = 2\Delta$. In this model, described in the inset of Fig. 3, the functional form of the magnetic susceptibility is written as, $\chi(T) = \chi_0 - 2\mu_B^2 \int N(E) \frac{\partial f(E,T)}{\partial E} dE$. Least square fitting of the polycrystalline average, $\chi_{avg.} = (\chi_a + \chi_b + \chi_c)/3$ yields $\Delta = 35.76 \pm 0.41$ meV, $W = 27.91 \pm 1.35$ meV and $\chi_0 = 2.2 \times 10^{-5}$ emu/mole which agree well with the reported results [6,7]. Figure 4 shows the electrical resistivity $\rho(T)$ of $FeSb_2$ single crystals along the three principal crystal axes against temperature. Qualitatively identical semiconducting behaviors were observed along the three axes up to 300 K.

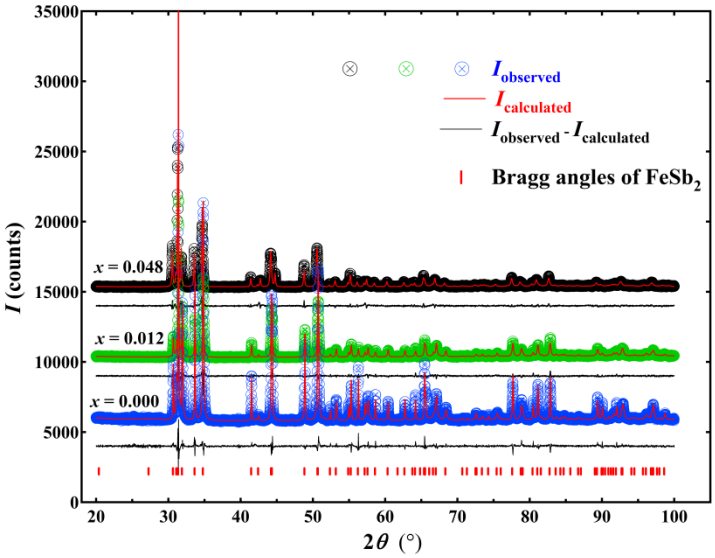

Figure 1. (Color online) Powder XRD patterns of $Fe_{1-x}Mn_xSb_2$ for representative x with the fitting results using the Rierveld method. The differences between experimental and fitting results are denoted in black solid lines. The positions of Bragg angles for $FeSb_2$ are indicated by red vertical bars. For clear visibility, the XRD patterns of x = 0.012 and x = 0.048 are vertically shifted.

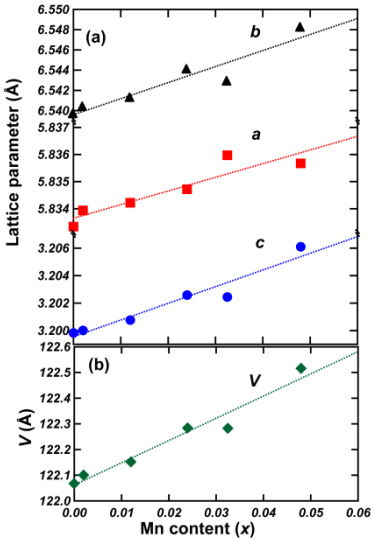

Figure 2. Mn concentration dependence of (a) the lattice parameters and (b) unit cell volume of $Fe_{1-x}Mn_xSb_2$.

Table 1: Refinement parameters, lattice parameters and atomic position parameters of Sb, x and y, refined by the Rietveld analysis of XRD patterns at room temperature using TOPAS. The marcasite phase with space group *Pnnm* and atomic positions of Fe/Mn at (0,0,0) and Sb at (x,y,0) are assumed (see text).

	x = 0.0	x = 0.002	x = 0.012	x = 0.024	x = 0.032	x = 0.048
R_{exp}	2.88	3.04	4.29	3.87	3.16	4.41
R_{wp}	4.44	7.66	7.65	9.02	7.53	8.76
R_p	3.40	5.33	5.87	6.30	5.33	6.46
$S = R_{wb}/R_{exp}$	1.54	2.52	1.78	2.33	2.38	1.99
a	5.8333(3)	5.834(3)	5.834(3)	5.835(4)	5.836(1)	5.836
b	6.5396(4)	6.540(3)	6.541(4)	6.543(5)	6.543(1)	6.548
c	3.1998(2)	3.200(2)	3.201(1)	3.202(2)	3.202(1)	3.206
x	0.1882(1)	0.1887(3)	0.1897(3)	0.1918(4)	0.1903(5)	0.18977
y	0.35582(9)	0.3565(2)	0.3563(2)	0.3564(3)	0.3555(3)	0.35608

The observed saturating behavior below 5 K and the anomaly at ~ 40 K are probably extrinsic due to a very small amount of impurities. As reported previously [3,5], two energy-gap behavior was observed. This two-gap behavior is interpreted as a manifestation of a temperature-dependent DOS, a gap-forming, in the electron-correlation driven semiconductor. The energy gaps ε_{g1} and ε_{g2} are estimated by the linear fits in the ln(ρ) vs 1/T plot (Arrhenius plot), shown in the inset of Fig. 4, in the temperature

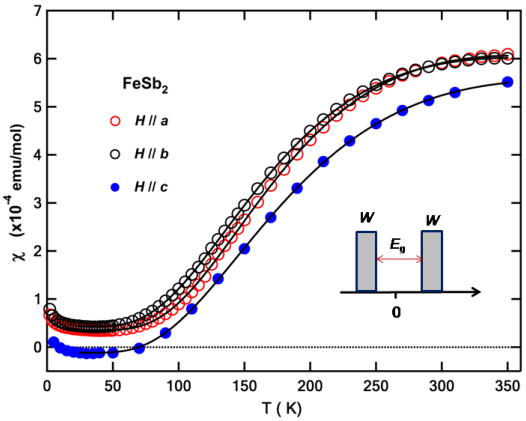

Figure 3. Temperature dependences of the magnetic susceptibility of $FeSb_2$ measured at H = 0.1 T applied along principal axes. The solid lines are fitting results based on the narrow-band small-gap model. Inset shows a schematic drawing of the DOS of the model.

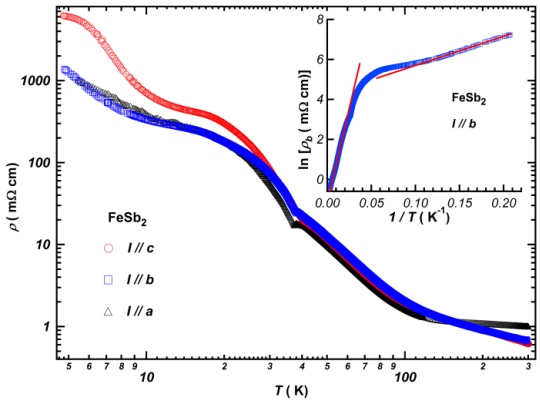

Figure 4. Electrical resistivity $\rho(T)$ of $FeSb_2$ for current applied along the three crystal axes. Inset shows the Arrhenius plot of $\rho_b(T)$ data in b direction and solid lines represent the linear fits (see text).

ranges T = 5 - 10 K and T = 50 - 120 K, respectively. The obtained values of ε_{g1} and ε_{g2} are about 2.5 meV and 33 meV, respectively, which are consistent with reported values [3,5]. The observed magnetic and electronic transport properties indicate a quality of our single crystals of $FeSb_2$ as high as in refs. 3, 5, 6.

We show the temperature dependences of the electrical resistivities of $Fe_{1-x}Mn_xSb_2$ single crystals along the b-axis in the form of Arrhenius plot in Fig. 5. The resistivity ρ_b is strongly reduced with increasing of the Mn-concentration at low temperatures. Especially, drastic change of ρ_b is found around $x \sim 0.01$, where ρ_b is reduced in two orders of magnitude. We estimate the gap energies ε_{g1} and ε_{g2} at low and high temperatures, respectively, by linear fitting. The slope in the high temperature region is almost not affected by the Mn-substitution, whereas the slope at low temperature is reduced continuously and becomes negative with increasing the Mn concentration. These variations indicate

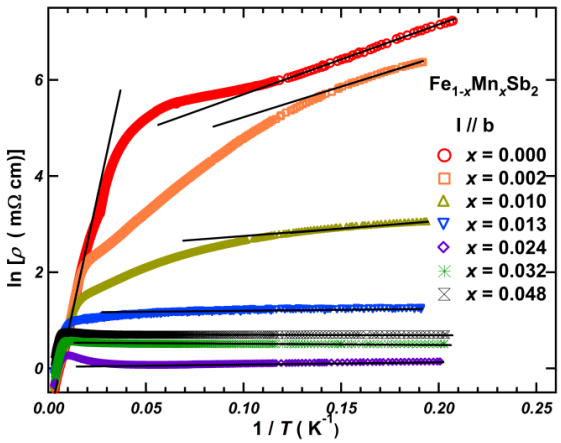

Figure 5. Electrical resistivity presented as Arrhenius plots of $Fe_{1-x}Mn_xSb_2$ single crystals for current applied along b direction.

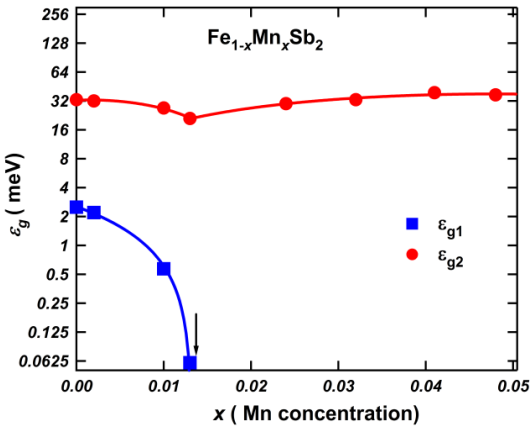

Figure 6. Mn concentration-dependence of the two energy gaps ε_{g1} and ε_{g2} in $Fe_{1-x}Mn_xSb_2$. Solid lines are guides to eyes and the vertical arrow indicates the critical Mn concentration of the small gap closing.

the drastic change of the resistivity is attributed to continuous reduction and disappearance of the smaller energy gap ε_{g1}. The negative slope above $x > 0.013$ indicate an emergence of the density of states (DOS) at the Fermi level and a metallic ground state upon the Mn-substitution. Estimated ε_{g1} and ε_{g2} are plotted against the Mn-concentration in Fig. 6. The small energy gap ε_{g1} decreases upon the Mn-substitution and closes completely just above $x = 0.013$ before the emergence of the metallic state at higher Mn concentrations. ε_{g2} slightly decreases first up to $x = 0.013$ then slightly increases by the Mn doping for samples showing metallic behavior at low temperatures. The observed electronic transport properties of $Fe_{1-x}Mn_xSb_2$ indicate that the metallic ground state induced by the Mn-substitution, corresponding to hole doping, in $FeSb_2$ semiconductor as well as by the electron-doping in the Co-substituted system, is attributed to the closing of the smaller energy gap ε_{g1}.

4. Conclusion

Single crystals of $FeSb_2$ and its Mn-substituted $Fe_{1-x}Mn_xSb_2$ for $x < 0.05$ were grown out of Sb flux. The successful and systematic Mn-substitution was indicated by XRD measurements and Rietveld analysis. Two energy-gap behavior in the resistivity and drastic suppression of the smaller gap by the Mn-substitution were found. The emergence of metallic state in $Fe_{1-x}Mn_xSb_2$ is due to the closing of the small energy gap of $FeSb_2$.

Acknowledgments

M.A.K. would like to thank the Ministry of Higher Education, Egypt for financial support during his PhD study.

References

[1] Aeppli G and Fisk Z 1992 *Comments Cond. Mat. Phys*. **16** 155
[2] Petrovic C, Kim J W, Bud'ko S L, Goldman A I, Canfield P C, Choe W and Miller G J 2003 *Phys. Rev.* B **67** 155205
[3] Bentien A, Johnsen S, Madsen G K H, Iversen B B and Steglich F 2007 *Europhys. Lett.* **80** 17008
[4] Holseth H and Kjekshus A 1969 *Acta Chem. Scand.* **23** 3043
[5] Sun P, Oeschler N, Johnsen S, Iversen B B and Steglich F 2010 *Dalton Trans.* **39** 1012
[6] Koyama T, Fukui Y, Muro Y, Nagao T, Nakamura H and Kohara T 2007 *Phys. Rev.* B **76** 073203
[7] Hu R, Mitrović V F and Petrovic C 2006 *Phys. Rev.* B **74** 195130
[8] Hu R, Mitrović V F and Petrovic C 2009 *Phys. Rev.* B **79** 064510
[9] Bruker AXS 2008 *TOPAS V4: General profile and structure analysis software for powder diffraction data. - User's Manual* (Karlsruhe: Bruker AXS)